PERGAMON

Deep-Sea Research II 49 (2002) 3957–3981

DEEP-SEA RESEARCH
PART II

www.elsevier.com/locate/dsr2

Large-scale sea-level variations and associated atmospheric forcing in the subtropical north-east Atlantic Ocean

Dimitrios Efthymiadis[a,b], Fabrice Hernandez[a,*], Pierre-Yves Le Traon[a]

[a] *CLS/Space Oceanography Division, 8-10 rue Hermes, 31526 Ramonville St-Agne, France*
[b] *Laboratory of Electromagnetism and Space Research, Demokritos University of Thrace, 67100 Xanthi, Greece*

Received 30 April 2000; received in revised form 25 June 2001; accepted 11 September 2001

Abstract

The large-scale sea-level variations in the subtropical north-eastern Atlantic Ocean are characterised by a predominant seasonal fluctuation. Analysis of 6 years (1993–98) of combined TOPEX/POSEIDON and ERS-1/2 altimetric data together with data of concurrent oceanic surface geophysical fields (ECMWF net heat fluxes, ECMWF winds, and Reynolds sea-surface temperature) reveals that the dominant physical forcing of sea-level variations on an annual timescale is the air–sea net heat fluxes. This local forcing generates a seasonal ocean steric response, whose amplitude (of the order of 4–5 cm) varies spatially within the studied area and temporally over the 6-year period. The residual variability is mainly characterised by a non-seasonal signal, which is observed northwards of the Azores Current ($\sim 34^{\circ}$N), and its time variation resembles that of the North Atlantic Oscillation (NAO). A combination of steric effects (wind-induced heat fluxes) and wind effects (barotropic Sverdrup response) appear to explain this signal. Some evidence of a local Ekman pumping response is also found regionally, both in the seasonal and non-seasonal variations of the observed sea level. At the interannual timescale, an overall sea-level trend with a mean rate of 0.5 cm/year is detected. However, the magnitude of the trend varies locally, so that the entire sea surface appears to undergo a general tilt, which extends beyond the studied area. Superimposed on this long-term trend, a sharp temporal sea-level rise occurs in 1995, mainly between the Azores and Madeira Islands. All together, these low-frequency sea-level variations seem to co-vary with the large-scale sea-surface temperature (SST) variations. This implies a comparable evolution of the sea level with the upper-ocean thermal content, which suggests a contribution from steric effects. A weaker situation is observed in the northern area, indicating a possible low-frequency wind-forcing-enhanced contribution.

Keywords: Sea-level variations; Satellite altimetry; Air–sea interaction; Seasonal variations; Long-term changes; Upper ocean

1. Introduction

Heat-flux exchanges between the upper ocean and the overlaying atmosphere are principally responsible for the large-scale sea-level variations of the mid-latitude global ocean at seasonal timescales (Gill and Niiler, 1973). Wave propagation also contributes significantly to the observed sea-level variations, in particular in the tropics (e.g., Chelton and Schlax, 1996). Baroclinic waves modify both the upper-ocean heat content and the sea level. Moreover, the large-scale sea-level

*Corresponding author. Tel: +33-561-394790; fax: +33-561-751014.
E-mail address: fabrice.hernandez@cls.fr (F. Hernandez).

0967-0645/02/$ - see front matter
PII: S0967-0645(02)00137-6

changes also can originate from steric response due to horizontal heat advection induced by strong currents, which, for instance, may be associated with seasonal changes of current paths (e.g., Kelly et al., 1999), from buoyancy forcing due to evaporation/precipitation processes, and from forcing by the fluctuating component of the surface wind (Willebrand et al., 1980).

Studies of sea-level variations in the subtropical north-eastern Atlantic have focused on mesoscale activity, which represents the most energetic scale of oceanic motion (e.g., Le Traon, 1991; Stammer et al., 1991; Tokmakian and Challenor, 1993; Le Traon and De Mey, 1994; Hernandez et al., 1995; Cromwell et al., 1996; Cipollini et al., 1997). The large-scale variability of this area has been studied mainly within the scope of global investigations. Wunsch (1991), using multi-channel regression analysis, found that between 40°W and 20°W, wind forcing could explain 50% of the GEOSAT-observed sea-level variance (with no correction of the inverse barometer effect) at 40°N, but the explained variance dropped to only 10–15% farther south ($\sim$20°N). Stammer (1997) has shown that for Atlantic basin-wide zonal averages the steric response calculated from European Centre for Medium-Range Weather Forecast (ECMWF) net heat fluxes can explain most of the TOPEX/POSEIDON (T/P)-observed seasonal sea-level variance, which increases in magnitude from the equator to the mid-latitudes (less clear farther north). This result has been re-examined recently by Ferry et al. (2000), who look into the North Atlantic at the T/P sea-level annual cycle in terms of steric effect due to heat fluxes, compared with other possible fluctuations at the seasonal scale. They demonstrate that the steric-height fluctuations as deduced from ECMWF net heat fluxes explain most of the sea-level seasonal cycle. To a lesser extent, the heat advection and the bottom pressure also contribute to the annual cycle, in particular in the Gulf Stream area. However, in the north-eastern Atlantic, 30% of the sea-level cycle could not be explained alone by the contributions mentioned. The remaining signal could correspond to the cumulated uncertainties of the altimetric measurements and modelled heat fluxes.

At longer timescales (decadal and interdecadal), Ezer (1999), in a model study of the North Atlantic subtropical gyre using realistic atmospheric forcing from 1950 to 1989, concludes that (a) the ocean responds linearly to the combined effect of SST and wind-stress anomalies, and (b) the western basin and the Gulf Stream system are affected by the low-frequency, westward-propagating Rossby waves generated in the eastern basin.

Thus, although the large-scale variability of the Atlantic Ocean has been already documented, studies have not clearly quantified the various fluctuations. As part of the CANIGO project, we investigate the large-scale variations of the ocean circulation in the subtropical north-eastern Atlantic (see Fig. 1) using the available accurate altimetric dataset and other datasets for the atmospheric forcing. The analysis focuses on the seasonal and interannual components of altimetric-observed sea-level variations in 1993–98, comparing them with atmospheric-induced sea-level changes deduced from the net heat fluxes and the wind fields. The spatial scales considered here are structures that exceed the dimensions of the oceanic eddies and the mesoscale turbulence (over 300 km). In particular, the study aims to address the following questions: What part of the large-scale sea-level variations can be explained by local heat-forced steric effects? What are the effects of the wind forcing? Are the large-scale sea-level variations in Sverdrup balance in the eastern part of the Atlantic subtropical gyre? Is there any ocean large-scale response to local Ekman pumping effects?

2. Data and processing

2.1. Altimetry

Using sea-surface heights (SSH) provided by the TOPEX/POSEIDON (T/P), ERS-1, and ERS-2 satellites, 6 years (1993–98) of sea-level anomaly (SLA) maps have been produced in this study. Several steps were necessary to obtain these maps. The data include: first, October 1992–December 1998 SSH of T/P reprocessed Merged GDRs (GDR-M Version C), distributed by AVISO

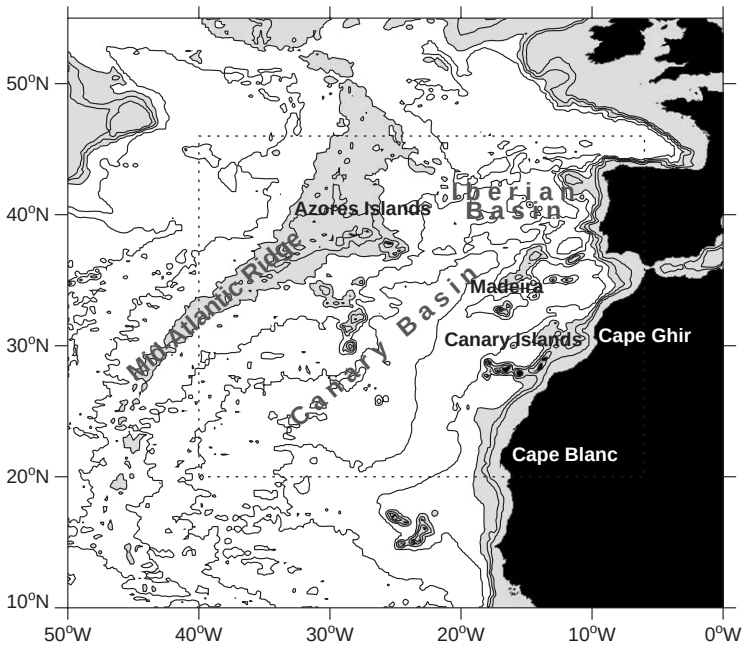

Fig. 1. Limits of the studied area, together with the bathymetry. Isobaths are plotted every 1000 m. Shallow areas (depth <3000 m) are shaded.

(AVISO, 1996); then phase C (October 1992–December 1993) and phase G (April 1995–May 1996) ERS-1 SSH; and finally, June 1995–December 1998 ERS-2 SSH from OPRs, distributed by CERSAT (CERSAT, 1994; CERSAT, 1996). In order to combine the 35-day repeat cycle ERS-1/2 data with the 9.95-day repeat cycle T/P data, the ERS-1/2 SSH were processed using—where possible—the same altimetric corrections. Second, a global crossover adjustment of ERS-1/2 arcs using the more accurate T/P data was performed, significantly reducing the ERS-1/2 large-scale uncertainties (i.e. orbit errors), and improving the consistency of the datasets (for more details, see Le Traon and Ogor, 1998). Third, T/P, ERS-1 and ERS-2 along-track SLAs were computed using a classical repeat-track analysis. The final merging was obtained by determining T/P and ERS-1/2 SLA maps on a weekly basis. An improved objective analysis technique was implemented (Le Traon et al., 1998) to interpolate along-track SLAs on a regular grid spacing ($0.2^\circ \times 0.2^\circ$) over the 40–6°W, and 20–46°N area. Note that during the December 24, 1993–March 24, 1995 period, maps were produced using T/P data only, since ERS-1 was operating in non-repeating geodetic phases. A detailed analysis of 10-day global SLA maps based on this improved interpolation technique can be found in Ducet et al. (2000).

To investigate further the large-scale circulation from these maps, the next step was to filter out the small scales, in particular the eddy field and the mesoscale turbulence. Thus, the maps were spatially smoothed on a $1^\circ \times 1^\circ$ grid, by computing at each grid point the $7^\circ \times 5^\circ$ longitude and latitude spatial average of the SLA relative to a 6-year mean (1993–98). The efficiency of the applied smoothing is illustrated in Fig. 2, where the temporal variability of each set of maps—as given by the root-mean-square (rms) of the gridded SLA time series—is compared. The variability of the smoothed maps, of the order of 3–5 cm rms (Fig. 2b), is everywhere lower than the corresponding values in the original variability map, ranging from 4 to 14 cm rms (Fig. 2a). In particular, the mesoscale signature associated with the Azores Current (AC, found between 33°N and 35°N) and

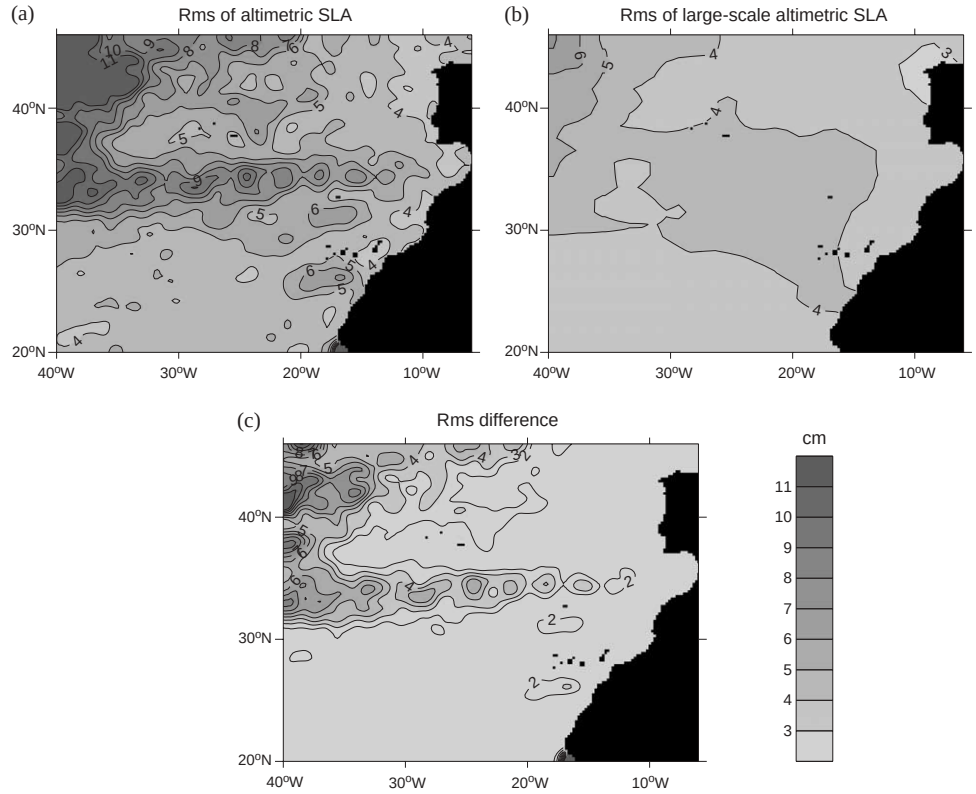

Fig. 2. Root mean square (rms) of altimetric SLA time series before (a) and after (b) a 3-month running average is applied. The difference of rms between (a) and (b) is given in (c). Contour intervals are in cm.

the southern branch of the North Atlantic Current (NAC, located in the north-western part of our studied area) has been wiped out at some points, as witnessed on the different maps (Fig. 2c) by the reduction of more than 2 cm rms. Thus, the most variable region of the smoothed SLA maps is located west of the Mid-Atlantic Ridge (MAR) (rms: 4–6 cm). The other active region (rms > 4 cm) is found in the central and northern part of the Canary Basin between the Azores, Madeira, and the Canary Islands. Weaker variability (rms < 3.5 cm) is observed around the Iberian Peninsula and near the northern African coast from Gibraltar to the Canary Islands.

The benefit of using combined ERS + T/P maps instead of only T/P maps to study the large-scale variability has been verified. Adding ERS data allows a more homogeneous spatial description of the mesoscale signal. Thus, the corresponding filtered maps are less possible to produce aliasing. Differences between filtered maps of T/P alone and filtered combined maps are 0.8–1 cm rms, distributed rather homogeneously over the studied area.

The next step was to perform a temporal smoothing, based on a 3-month running average performed at each grid point over the 6 years of weekly smoothed maps, in order to filter out the sea-level high frequencies associated with the mesoscale circulation. The time filtering applied retains the seasonal timescale and lower frequencies, which constitute the major part (~95%) of the SLA time-variance at large scales.

2.2. *Heat fluxes*

Net heat fluxes from the ECMWF were used to estimate the steric response of the ocean to local

heating/cooling. The wind fields, distributed as 5-day averages on a $1^\circ \times 1^\circ$ spatial grid, were re-interpolated to the 7-day grid of the SLA maps. The steric-height estimation is based on the assumption of a local balance between the net heat flux Q and the heat storage rate (HSR) on seasonal timescales (Gill and Niiler, 1973). Therefore, by ignoring the salinity and advection effects, the variation in time of the steric-height change, η_{St}, is approximated, to a first order, by a linear function of the net heat flux, $Q(t)$, after removing any non-zero net mean heat flux from the 6-year time series

$$\eta_{St}(t+1) = \frac{\alpha Q(t)}{\rho_0 c_p}\Delta t + \eta_{St}(t). \quad (1)$$

Here, $\alpha = -(1/\rho)(\partial\rho/\partial T)_{p,S}$ is the thermal expansion coefficient (ρ the seawater density and T the temperature at a specific depth), $\rho_0 \cong 1030\,\mathrm{kg/m^3}$ the mean density, $c_p \cong 3960\,\mathrm{J/kg\,K}$ the thermal capacity of seawater, and Δt the time interval (1 week). The coefficient α varies in space and time and depends on the thermohaline structure of the upper ocean. Within the studied area, it presents larger values in the southern part but exhibits a stronger seasonal variability in the central and northern parts (see Appendix A). A monthly time-varying α was computed, following the formula provided in Table 3.1 of Gill (1982), and using monthly temperature T and salinity S data of the upper 200 m of the ocean from the World Ocean Atlas 1994 (WOA94 hereafter, see Levitus et al., 1994).

Steric-height anomaly maps were then produced on a $1^\circ \times 1^\circ$ grid by first removing the 1993–98 temporal mean. The maps were spatially and temporally filtered in a similar way to the altimetric maps ($7^\circ \times 5^\circ$ spatial averaging, 3-month averaging).

2.3. Wind

In order to examine the large-scale ocean response to wind forcing, the ECMWF surface wind data were selected for the Canary basin. The accuracy of the wind data used was assessed by performing statistical comparisons with wind data products based on satellite scatterometry (from both the ERS-1/2 and NASA ADEOS-1/NSCAT scatterometers), which provide less energetic forcing, as described in Appendix B.

At timescales longer than 1 month, the ocean barotropic circulation is expected to be in Sverdrup balance with wind forcing. That is, the wind vorticity forcing is balanced by the advection of the planetary vorticity in the water column (Willebrand et al., 1980). The resulting SSH (η_{Sv}) is thus represented by the wind-forced barotropic streamfunction, which can be estimated by zonally integrating the wind-stress curl field, $\mathrm{curl}_z\,\vec{\tau}$, from the ocean basin eastern boundary

$$\eta_{Sv} = \frac{-f}{g\rho_0\beta}\int_{x_{east}}^{x} \frac{1}{H}\,\mathrm{curl}_z\,\vec{\tau}\,\mathrm{d}x. \quad (2)$$

Here, f, g, β, H, and τ are the Coriolis parameter, the gravitational constant, the beta-parameter ($2\omega\cos\theta R^{-1}$, with $\omega \cong 7.292 \times 10^{-5}\,\mathrm{s^{-1}}$ the angular speed of the earth, θ the latitude, and $R \cong 6371$ km the radius of the earth), the depth of the ocean, and the wind stress, respectively. We used the flat bottom topography approximation in the calculation (with a constant value of $H \cong 4$ km).

Moreover, a baroclinic response of the ocean to local wind forcing is also expected. Thus, the sea-level response due to local Ekman pumping was evaluated too, assuming a simple model of a two-layer ocean, with the deeper layer at rest. The corresponding Ekman SSH (η_{Ek}) was estimated by integrating in time the wind-stress curl field

$$\eta_{Ek} = -\frac{g'}{\rho_0 g}\int \frac{\mathrm{curl}_z\,\vec{\tau}}{f}\,\mathrm{d}t. \quad (3)$$

Here, $g' = g(\Delta\rho/\rho)$ where $\Delta\rho$ is the density difference between the upper and lower layers. The factor $\Delta\rho/\rho$ was set to 0.003. The Ekman response is expected to have a larger amplitude than the barotropic Sverdrup response at large spatial scales and seasonal timescales, especially at low latitudes (Gill and Niiler, 1973).

Finally, maps of the SLA caused by these two wind effects were estimated, by first removing the mean 1993–98 field, and then by filtering spatially and temporally as for the altimetric and steric-calculated maps.

2.4. Sea-surface temperature

Weekly mean SST data on a $1^\circ \times 1^\circ$ grid produced by Reynolds and Smith (1994) also were used in our study, because the SST can be used to infer the variability of the upper-ocean heat content, and therefore of ς_{St}, especially during winter, when the upper ocean is well mixed (White and Walker, 1974). The seasonal variation of the SST is correlated with the seasonal variation of the altimetric-observed sea level (e.g., Knudsen et al., 1996; Leuliette and Wahr, 1999). On interannual timescales, a strong correlation is also found between global maps of sea-level trends and SST trends (Chambers et al., 1997; Nerem et al., 1997; Leuliette and Wahr, 1999).

The spatial filtering ($7^\circ \times 5^\circ$ averaging) mentioned above was applied to all oceanic surface fields whenever the correlation analyses were performed. Nevertheless, when Empirical orthogonal function (EOF) analyses were performed, the altimetric sea-level maps were spatially filtered to study both the seasonal-scale and interannual-scale variations, while the other fields were spatially filtered only to study interannual variations. We proceeded as described above, in order to preserve the spatial characteristics of the seasonal-scale principal empirical modes, which, however, exhibit large-scale spatial patterns.

3. Seasonal sea-level variations

3.1. Altimetric observations

The dominant mode of SLA variability is the seasonal cycle (also referred to as the ''annual cycle''). The time series of the domain-averaged SLA undergoes a seasonal fluctuation with an amplitude of ~ 4.8 cm (Fig. 3a). The low-frequency (interannual) variation of the domain-averaged SLA, which appears as a near-linear trend superimposed on the seasonal fluctuation, will be discussed in Section 4. To focus on the sea-

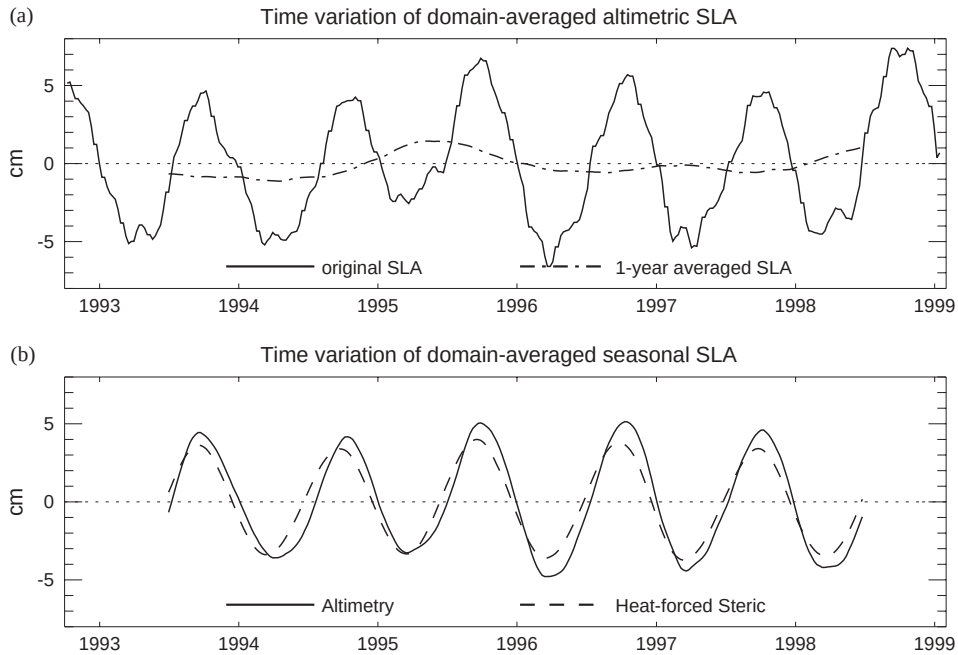

Fig. 3. Time variation of (a) the domain-averaged altimetry-observed SLA (solid) together with the result obtained after a 1-year running averaging (dashed–dotted), and (b) the seasonally filtered domain-averaged altimetric SLA (solid) and heat-forced steric SLA (dashed).

level seasonal variability, the low-frequency variation was filtered out by subtracting a 1-year running mean (note that high frequencies were reduced by applying a 3-month running mean, as described in Section 2.1). The time filtering applied—although not optimal—isolates the bulk seasonal variance of the SLA, namely the near-harmonic annual oscillation with its interannual modulation too. The spatial aspect of the seasonal variability, i.e. how it is geographically distributed throughout the area of study, was examined by applying an EOF analysis scheme to the seasonally filtered SLA time series of all points within the studied area.

The EOF decomposition of the seasonally filtered SLA yields primarily a standing annual oscillation with an average amplitude of ~4.3 cm (Figs. 4a and c), which explains most (94%) of the total variance, and exhibits a fairly stable pattern during the studied period (1993–98). Stronger amplitudes (larger than 4.5 cm) are found west of the MAR and in the central area of the Canary Basin, while weaker amplitudes (<4 cm) are observed west and north of the Iberian Peninsula. Moreover, an intensification of the amplitude is observed during the year 1995. From ~3.6 cm for the 1994/95 year, it reaches 5 cm during 1996 and then gradually decreases. We must note here that the average amplitude of the time-filtered SLA (~4.3 cm, Fig. 3b) is smaller than the original (non-time-filtered) one (~4.8 cm, Fig. 3a).

The EOF analysis of the original (non-time-filtered) SLA yields a principal empirical mode with spatial and temporal patterns (not shown) that are strongly correlated with the time-filtered SLA. Such correlation corroborates the dominant contribution of the seasonal-scale time variations that explains most of the large-scale altimetric SLA variance.

3.2. Heat-flux-induced SLA variations

The contribution of the heat-flux-induced steric-height variations to the altimetric-observed seasonal signal was examined by applying the same filtering scheme for the calculated steric-height maps in order to extract the seasonal-scale steric signal. The time series of the domain-averaged

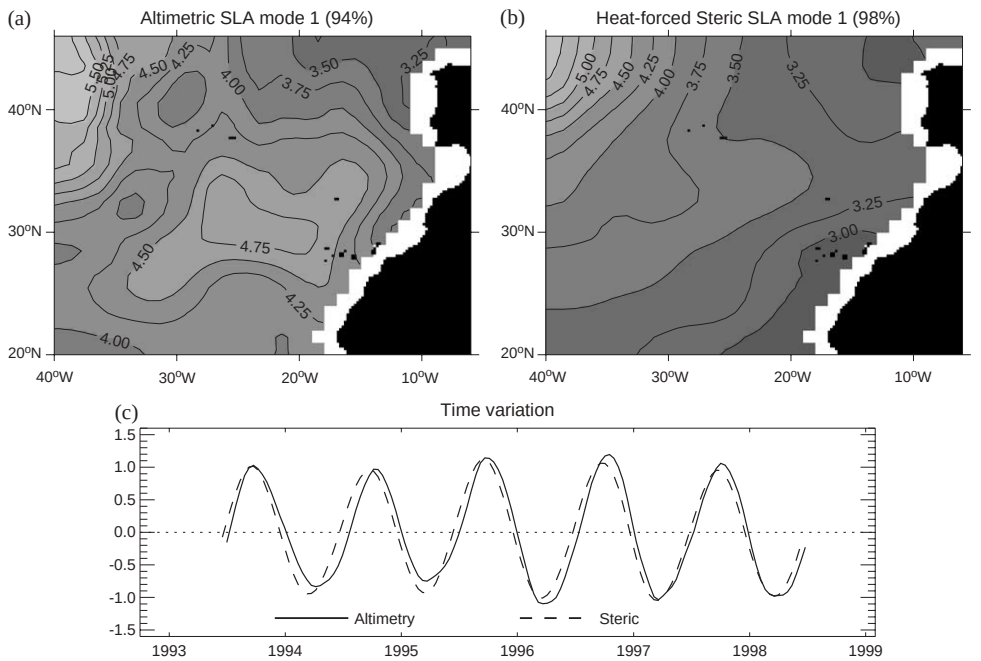

Fig. 4. Spatial patterns (a, b) and corresponding time variation (c) of the two principal empirical modes of the seasonally filtered, large-scale, altimetric and steric SLA. Contour intervals are 0.25 cm.

steric SLA_{St}, undergoes a seasonal oscillation closely related to the observed (altimetric) SLA (Fig. 3b), with a lead of ~ 2 weeks and slightly smaller amplitude. The correlation (r) of the altimetric SLA with the steric SLA is, in general, high ($r > 0.9$, after the SLA time series lagged by 2 weeks), although it is weaker north of 40°N, and on the western side of the MAR too (Fig. 5a). The calculated steric-height variation does not explain the observed sea-level variance in the same proportion throughout the studied area. A measure of the skill of this heat-flux-induced steric-height estimation in explaining the altimetric-observed signal is given by

$$\mathrm{Skill}_{\mathrm{steric}} = \left(1 - \frac{\mathrm{Variance}\ (\mathrm{signal}_{\mathrm{altim}} - \mathrm{signal}_{\mathrm{steric}})}{\mathrm{Variance}\ (\mathrm{signal}_{\mathrm{altim}})}\right) \times 100. \quad (4)$$

The computed skill exceeds 90% over most of the studied area (Fig. 5b). Lower skill values are found west of the MAR and, somewhat surprisingly, in the central and southern part of the eastern Canary Basin. On the other hand, in the Iberian Basin the skill is high, despite weaker correlation.

The principal empirical mode obtained from an EOF analysis of the seasonally filtered steric SLA_{St} (98% of the variance, seeFigs. 4b and c) has similar time variations to the referring altimetric SLA, although their spatial patterns are different. The spatial pattern of the steric SLA mode is characterised by gradually decreasing amplitude from northwest (5 cm) to southwest (3 cm), without the discontinuity in the altimetric SLA pattern (Figs. 4a and b). Another low-amplitude region appears west/northwest of the Iberian Peninsula.

To investigate further the part of the altimetric seasonal variations not explained by the heat-flux-induced steric SLA, the "altimetric-minus-steric" differences were computed at each grid point. In what follows, the time series obtained are called remnant SLAs*. An EOF decomposition was performed on this remnant signal. Its first mode, characterised by a quasi-annual oscillation in phase with the altimetric one, explains almost half (49%) of the total variance (Fig. 6b). This oscillatory mode has stronger amplitudes (over 1 cm, see Fig. 6a) in roughly the same areas where low skill of the estimated steric SLA_{St} was found (Fig. 5b). Thus, the first mode of the remnant signal reveals the heat-flux-induced SLA's inability to model correctly the steric-height variations observed by the altimetry at seasonal timescales. In other terms, the steric-height estimation is partially accurate, possibly because of inaccurate net heat fluxes. This possibility will be further examined when discussing the comparison with the wind-derived sea-level variations in the next subsection.

3.3. Wind-induced SLA variations

The contribution of wind forcing to the sea-level variation will be examined by comparing the

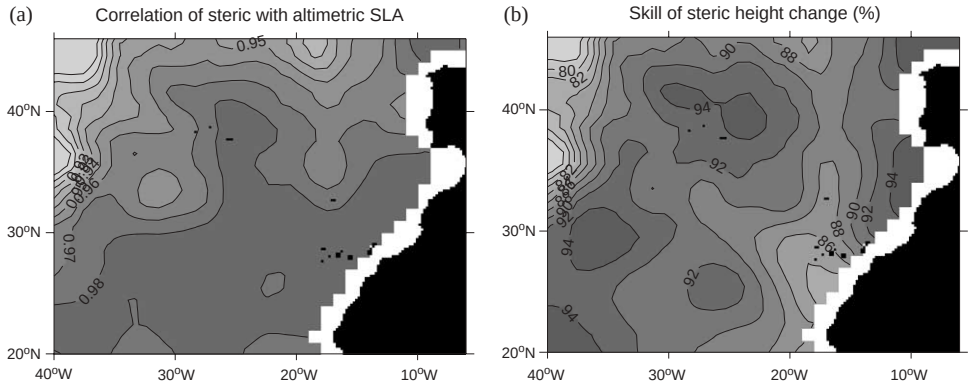

Fig. 5. Altimetric SLA in relation with heat-forced steric SLA: (a) correlation coefficient (for 2-week time lag of altimetric SLA), and (b) skill (percentage of explained variance) of the steric SLA.

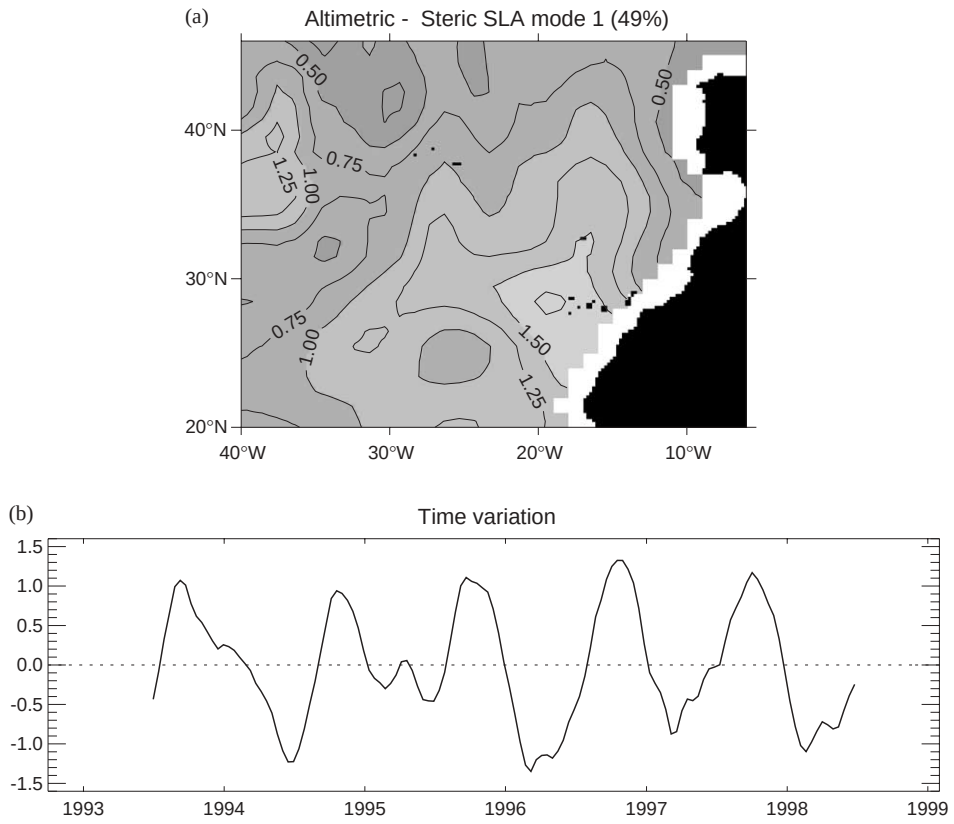

Fig. 6. Spatial pattern (a) and corresponding time variation (b) of the principal empirical mode of the remnant (altimetric–steric) SLA.

remnant SLA* signal with the calculated sea level predicted by the Sverdrup model (SLA_{Sv}) and the Ekman pumping response (SLA_{Ek}). That is, focusing on the altimetric sea-level variations that are not explained by the heat-flux-induced steric-height variations. However, a straightforward comparison between the remnant SLA* and the Sverdrup SLA_{Sv} and Ekman SLA_{Ek} can lead to wrong conclusions, since the remnant SLA* seems to be dominated by a steric-like quasi-annual oscillation. For this reason, our approach will be a qualitative one.

3.3.1. Sverdrup balance

The remnant signal, apart from the steric-like component (Fig. 6), has a noticeable variance in the northern half of the studied area, where the wind-stress curl field exhibits strong variance with a dominating non-seasonal pattern (see Appendix C). The term 'non-seasonal' is used here to express the signal variation that cannot be modelled as a superposition of an annual and a few sub-annual harmonics. We have thus attempted to examine the contribution of wind forcing using the EOF decomposition of the altimetric, steric, and wind-induced (Sverdrup model) signals.

Prior to the EOF decomposition, the principal empirical modes of the altimetric and steric SLAs, which largely explain the seasonal variations (see Fig. 4), were, respectively, subtracted from both signals. Because the variance of the residual signal (i.e. what remains after the subtraction) is not uniformly distributed throughout the studied area (especially in the case of the altimetric signal), the covariance matrix of the SLA maps was computed once the SLA time series of every geographical point had been normalised with their respective standard deviation (direct estimation of the

empirical modes without this normalisation provides patterns biased towards the most energetic regions, located on the northwestern side of the studied area).

The patterns of the resulting principal empirical modes of the residual altimetric and steric SLAs seem to compare well in time ($r \sim 0.76$) and to a lesser extent in space (Fig. 7). The altimetric mode spatial pattern appears to have strong-to-low magnitudes from the north to the south, separated by a tight meridional-gradient zone. Close to the Iberian Peninsula the gradient zone has an almost meridional orientation (zonal gradient), following the coastline. The steric mode is characterised by a continuous pattern crossing the studied area, forming a similar spatial gradient at its southeastern side with the altimetric one, while it is quite different at the northwestern side. We should stress at this point that an empirical mode, with similar spatial and temporal patterns, also can be obtained if we apply the EOF analysis directly to the altimetric-minus-steric SLA. In this case, however, the empirical mode obtained is ranked second (based on explained variance) due to the dominating steric-like principal mode (Fig. 6).

Nonetheless, part of the residual altimetric SLA variance exhibited in its principal empirical mode can be also explained by a wind-induced response. The correlation in time between the residual altimetric SLA principal mode (Figs. 7a and c) and the principal mode of the Sverdrup SLA_{Sv} is quite high ($r \sim 0.65$). Moreover, to reduce the possible residual contribution of the heat fluxes on the sea-level variations, we subtracted the residual steric principal mode (Figs. 7b and c) from the residual altimetric signal and then applied an EOF analysis (on the normalised signal). The calculated principal empirical mode now correlates better in time ($r \sim 0.70$) with the principal empirical mode of the Sverdrup SLA_{Sv} (Fig. 8). The spatial pattern of the SLA_{Sv} exhibits a similar meridional gradient in the middle of the studied area, which becomes zonal west of the Iberian Peninsula. Nevertheless, it has an unrealistic continuous increase in magnitude towards the northwestern side. We should note that the correlations mentioned above

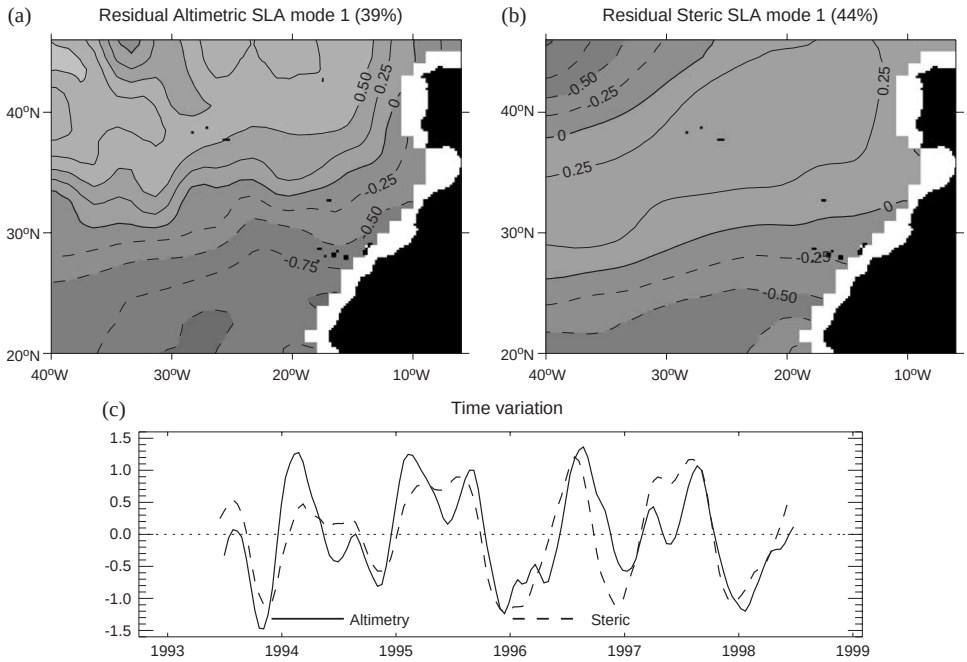

Fig. 7. Spatial patterns (a, b) and corresponding time variation (c) of the empirical modes of the residual altimetric and residual steric SLA. The residual signal represents the original signal without its principal empirical mode (see Fig. 4).

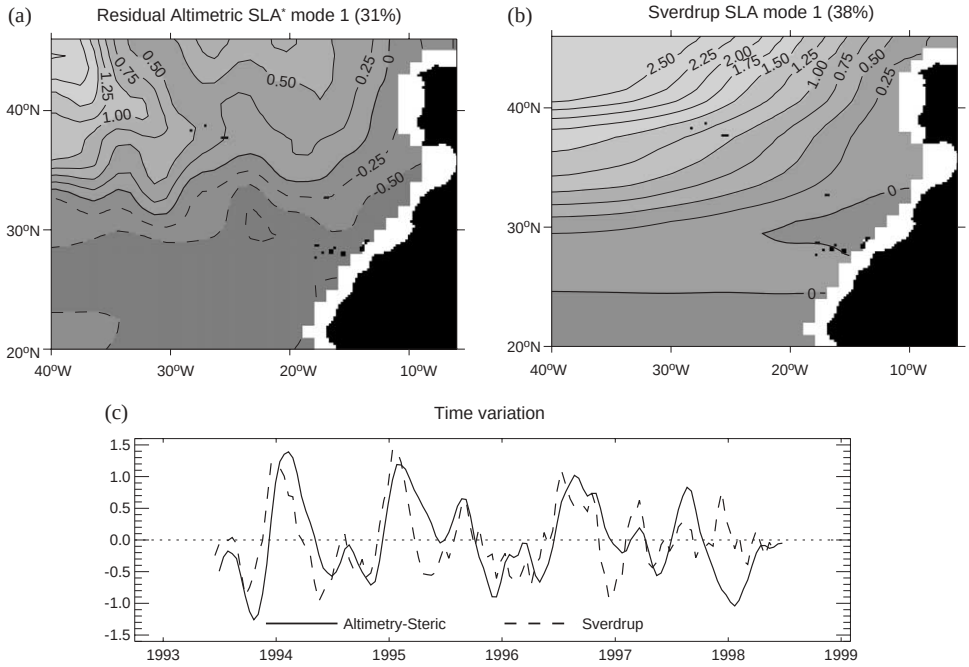

Fig. 8. Spatial patterns (a, b) and corresponding time variation (c) of the empirical modes of the residual altimetric SLA and the Sverdrup SLA. The signal, which corresponds to the residual steric SLA mode 1 (Figs. 7b and c), has been removed from the residual altimetric SLA before the EOF decomposition.

correspond to a 2-week time lag of the altimetric SLA in relation to the Sverdup SLA, which, in the context of a lead-lag analysis performed, gave the higher correlations.

3.3.2. Ekman pumping

Lastly, the possible contribution of Ekman pumping effects to the seasonal-scale variability is examined in this subsection. It is expected to be complementary to the steric-height changes at specific regions, in particular wherever the remnant SLA* signal exhibits anomalous high or low amplitudes.

We start by performing a specific time filtering on the altimetric, steric, and Ekman pumping SLA in order to better estimate the seasonal component. This includes: (a) extracting the annual component by fitting the 6-year (long) signal with annual harmonics within a 1-year time-running window, after removing the 1-year linear trend; (b) fitting the residual signal, namely the non-time-filtered minus the annual component, with semi-annual harmonics within a 6-month time-running window (the 6-month linear trend is again removed, prior to the fitting); and (c) summing the resulting annual and semi-annual components.

Surprisingly, the correlation analysis between the remnant (steric-corrected) SLA* and the Ekman pumping SLA_{Ek} (not shown) indicates that the correlation coefficient (wherever it exhibited noticeable values) was further increased if the amplitude of the steric SLA_{St} was considered 10% larger than what was initially estimated. This implies a possible underestimation of the steric-height amplitude. After assuming that the SLA_{St} was underestimated by that ratio, we attempted to calculate the skill of the Ekman pumping in explaining the non-steric part of the signal. Because the datasets from the ECMWF and CERSAT centres exhibited differences, in particular in the Canary Islands region (see Appendix B), we used both sources to enhance the reliability of the results. The ECMWF data gave the pattern with the higher correlation. The results are

presented in Fig. 9 together with plots of the SLA time variation at selected high-correlated points. Two regions in the north appear to have good skill (> 20%), while two others with less skill are found east of the Madeira Island and northwest of the Cape Blanc. However, the resulting values in the region off the northwest Africa were not confirmed by the CERSAT wind-based signal. We note that the northeastern region coincides with the centre of action related to the North Atlantic Oscillation (NAO; see Appendix C).

4. Interannual variations

On interannual timescales, the local balance between the HSR and the ocean–atmosphere heat exchanges will be less valid due to heat advection

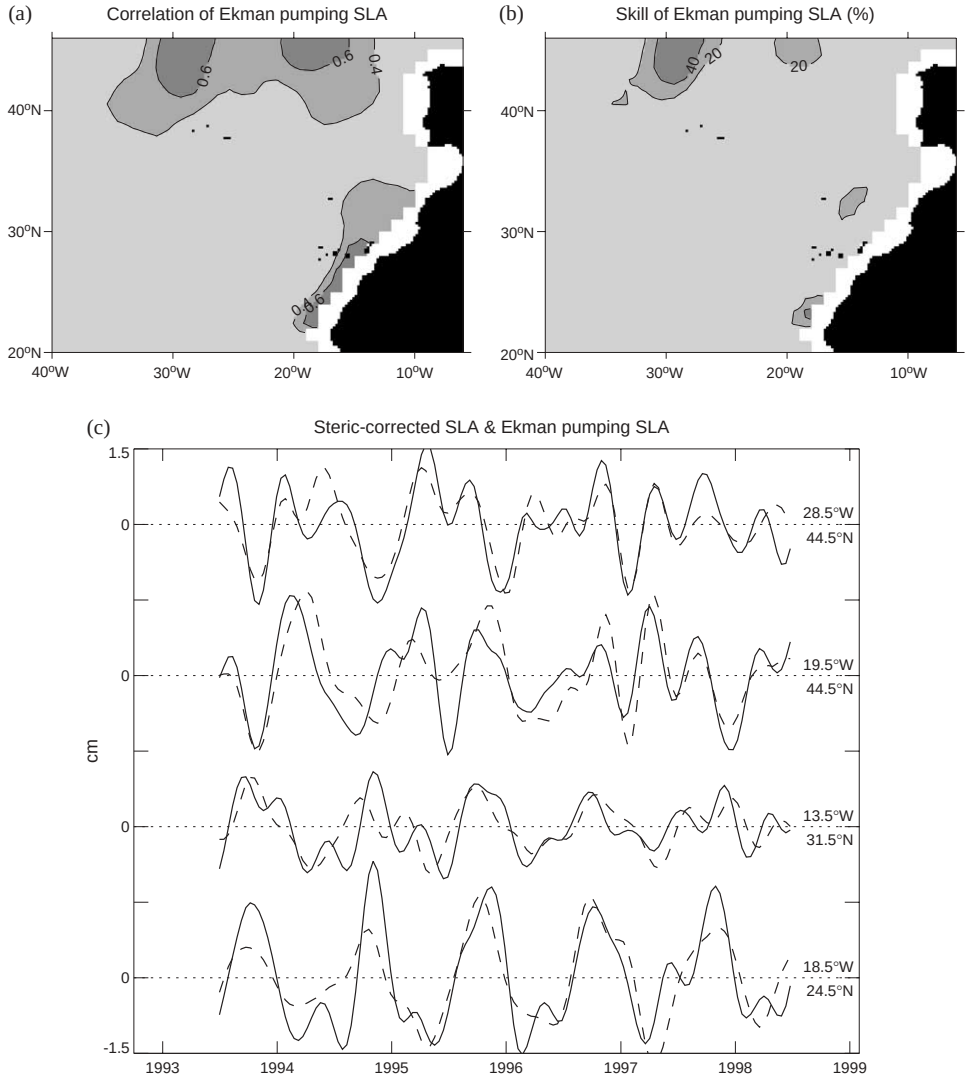

Fig. 9. Steric-corrected SLA in relation to Ekman pumping SLA: (a) correlation coefficient, and (b) skill (i.e. percentage of explained variance) of Ekman pumping SLA. Plots of the time variation of steric-corrected and Ekman pumping SLA from selected points among the most correlated patterns are given in the bottom panel (c).

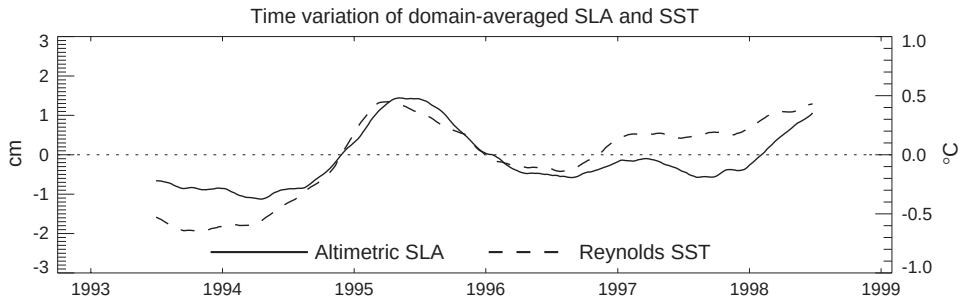

Fig. 10. Interannual variability of the domain-averaged SLA (solid), and the domain-averaged SST (dashed), respectively, scaled on the left and right axis.

caused by the ocean currents. However, the SST data can be considered as an approximate estimate of the upper-ocean heat content. This leads us to compare SST variability spatially and temporally with the sea-level changes on interannual timescales.

Prior to analysis, the SLA and SST time series were time-filtered, applying a 1-year running mean, in order to exclude the annual and subannual scale variations. The resulting domain-averaged SLA time series exhibits a continuous increase during 1993–98, with a mean rate of 0.5 cm/year (linear regression fit) and a superimposed maximum during 1995 (Fig. 10). The domain-averaged SST is characterised by a similar variation with an increase of 0.3°C/year (Fig. 10).

The spatial and temporal characteristics of the SLA–SST correlation were examined by performing an EOF analysis of the time-filtered signals in a widely extended domain (compared to the studied area). The near-linear trend of the domain-averaged SLA is reproduced mostly everywhere across the basin, but with locally alternating positive and negative signs. On the other hand, the maximum during 1995 is a rather local phenomenon, which is predominantly evident in the studied area. It is therefore reasonable to assume that different dynamical sources are responsible for these two distinct interannual variations. Thus, we adopted the following analysis strategy: the EOF decomposition was performed (a) on detrended signals, and (b) on signals from which the variation corresponding to the principal empirical mode obtained from stage (a) is removed.

The principal empirical modes for both the detrended SLA and SST account for more than 60% of the total variance and mainly represent the temporal rise of sea-surface height and temperature during the year 1995. Their spatial patterns (Figs. 11a and b) and the time variation of the relative amplitudes (Fig. 11d) are quite similar. The maximum variation is observed in the area between the Azores and Madeira, although it is located closer to the Azores Islands in the SLA field than the SST one. The northwestern corner of the area also exhibits some differences.

Empirical modes of SLA and SST computed after subtracting from each field the variation associated with the above-mentioned empirical modes (stage (b) of our analysis) clearly characterise the large-scale temporal linear trend in both signals. Their respective temporal patterns are fairly similar (Fig. 12c). However, their spatial patterns are mainly comparable with that of south of 35°N (Figs. 12a and b). The SLA pattern exhibits a sea-level fall on the northwestern side and a rise on the southeastern side. The spatial amplitudes of the SST mode are almost everywhere positive (indicating an SST increase). In addition, the linear regression fit on the original fields yields trends with values spanning from 1 cm/year (west of the Gibraltar Strait) to −0.5 cm/year (northwest of the Azores Islands). The SST trend ranges between 0.2 and 0.4°C/year. Consequently, the ratio between the SLA and SST trend varies regionally (−2.4 to 3.5 cm/°C). The maximum value of the SLA-to-SST trend appears off the Gibraltar Strait (3.5 cm/°C). We note here that the linear trend characterises mainly the period

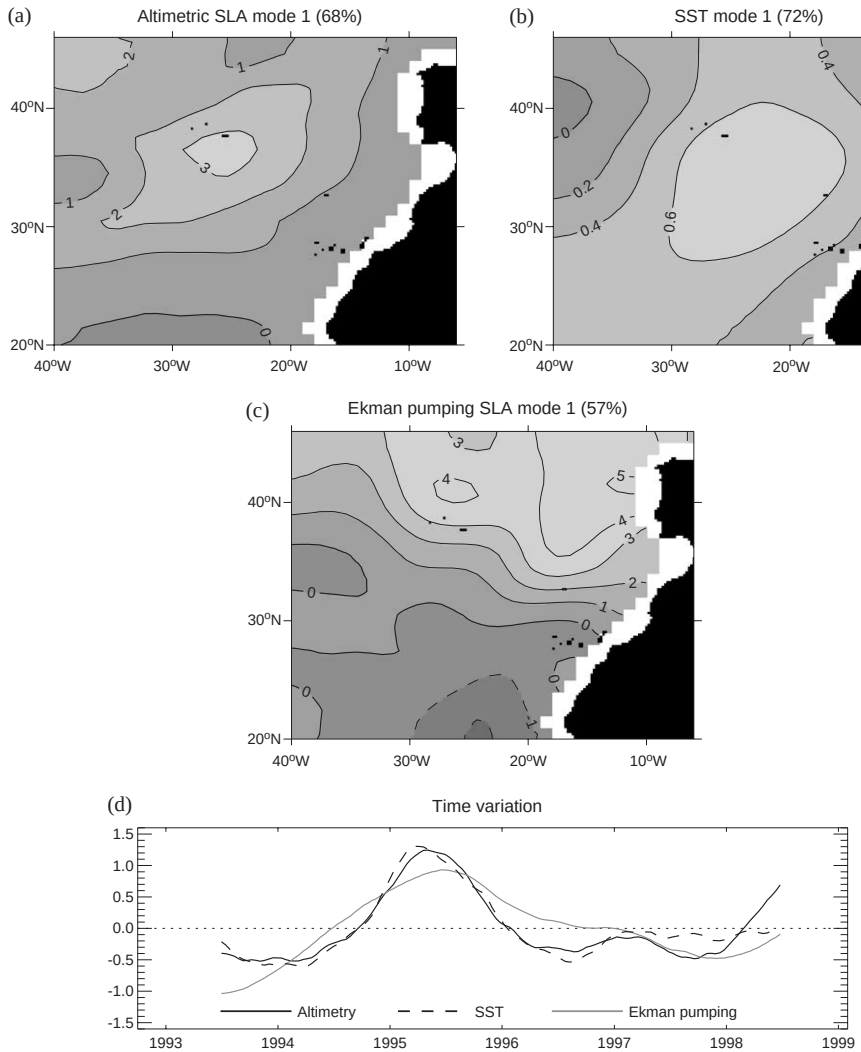

Fig. 11. EOF analysis of the detrended interannual altimetric SLA, SST, and Ekman pumping SLA: spatial patterns of the principal empirical modes (a, b, c) and the corresponding time variation (d). Contour intervals are 1 cm (SLA) and 0.2°C (SST).

between mid-1994 and mid-1998. Before that, and perhaps after that, a nearly opposite variation took place. Higher-order empirical modes correspond to a variance below 10% and are not examined.

Lastly, we examined the contribution of wind forcing in the interannual sea-level variation by applying the EOF analysis on the time-averaged (1-year running mean) time series of both "Sverdrup" and "Ekman" SLAs, computed according to the Sverdrup and Ekman pumping models (Section 2.3). In fact, the resulting principal empirical modes of Sverdrup and Ekman pumping SLA are both based on the low-frequency component of the wind-stress curl principal empirical mode (see Appendix C), which is related to the NAO interannual variability. The principal mode of Sverdrup SLA (69% of the total variance) has a spatial pattern similar to Fig. 8b. The corresponding time variation is chiefly developed during 1995

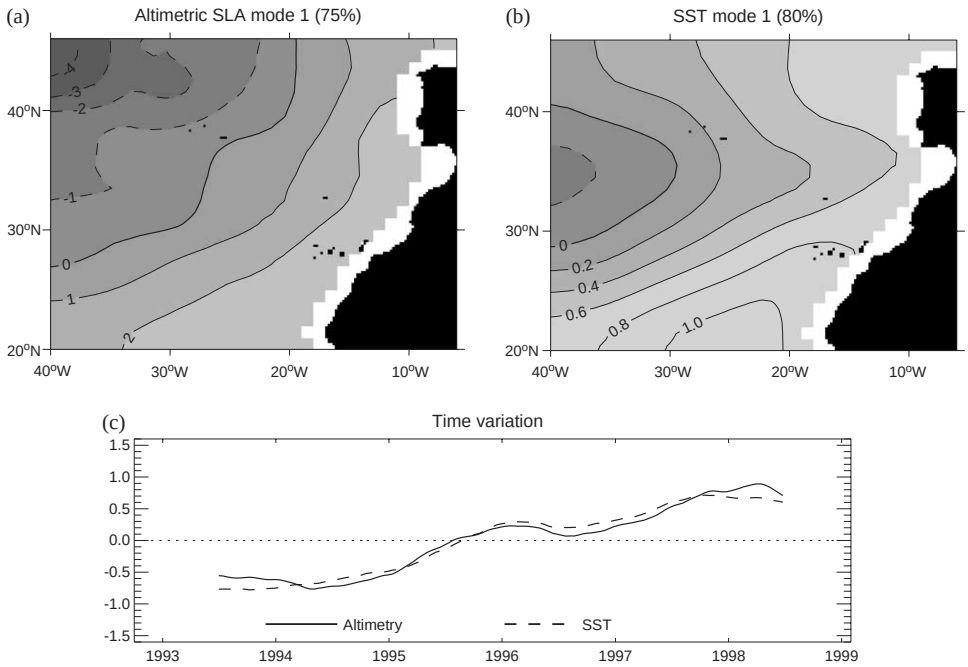

Fig. 12. EOF analysis of the interannual altimetric SLA and SST for which the variability associated with the principal mode (presented inFigs. 11a and b) has been subtracted: spatial patterns of the principal empirical modes (a, b) and the corresponding time variation (c).

through a change of sign manifesting a change in the zonal sea-level gradient in the region north of the Azores Current. This represents the low-frequency component of the Sverdrup SLA (modulated mainly by the winter conditions), which was removed when analysing the seasonal-scale variability. On the other hand, although the time variations of the principal modes of the detrended altimetric SLA and the Ekman pumping SLA are closely matching each other (Fig. 11d), their respective spatial patterns are quite different (Figs. 11a and c).

5. Discussion

The large-scale sea-level variability at seasonal timescales in the northeastern subtropical Atlantic Ocean is mainly associated with the seasonal changes of the upper-ocean heat content. This is a characteristic of the extra-tropical latitudes well noticed in altimetric studies (Han and Ikeda, 1996; Wang and Koblinsky, 1996; Isoguchi et al., 1997; Stammer, 1997; Fukumori et al., 1998; Vivier et al., 1999). In the investigated area, the annual SLA variation revealed by altimetry has an average amplitude of $\sim$4.8 cm, reaching maximum (minimum) height in late October (late March). The steric height, derived from ECMWF heat fluxes, can explain the most of the large-scale altimetric SLA. A quasi-annual residual oscillation is found, with noticeable amplitude (more than 1 cm) in the ocean surrounding the Canary Islands (Fig. 6). We could not explain this oscillation, although other forcing suggests that the steric response derived from ECMWF net heat fluxes is underestimated. Indeed, in this region there is no strong wind-stress curl annual variation, and the salinity contribution to the steric effect is expected to be negligible, except (a) in the ocean near the Iberian Peninsula where considerable seasonal river water outflows, and (b) in the Gibraltar area where the Mediterranean water outflow can modify the salinity of the ocean. Our steric-height calculation uncertainties

are another possible source of error (Eq. (1)). The impact of the assumptions on the thermal expansion coefficients were assessed by computing steric heights (following Eq. (1)) with α estimated over different depth ranges, from the surface to the 200-m upper layer. The domain-averaged, seasonally filtered SLA (annual amplitude $\sim$4.3 cm) is better fitted when thinner layers are taken into account to compute α: the steric-induced annual amplitude equals $\sim$3.6 cm for a 200-m layer computation, whereas it equals $\sim$3.9 cm for an unrealistic surface-only computation. That is, a 10% reduction of the annual fit. Thus, the most probable source for the observed deviation in the steric-height computation remains the underestimation of the net heat flux variation in the ECMWF data, as argued by Wang and Koblinsky (1997). Its influence has also been widely discussed by Ferry et al. (2000) for the Atlantic Ocean area. They show that heat flux uncertainties of 35 W/m^2 are expected, which imply steric-height seasonal amplitude misfits of the order of 0.5–1 cm in the area. On the other hand, contribution from steric effects of deeper ocean layers has been evidenced only off the northwestern Iberian Peninsula (Ferry et al., 2000).

The interannual variation of the annual cycle's amplitude appears to be associated principally with the variation in the magnitude of the sea-level fall during winter. The sea-level fall is in turn dependent on the net heat loss, which takes place mainly during the late autumn to early winter period (November–February). The domain-averaged net heat loss was quite small ($\sim$106 W/m^2) during the end of 1994, while it reached its maximum—for the 1993–98 period—($\sim$141 W/m^2) during the end of 1995. The reduced sea-level fall ($\sim$7.4 cm) during the winter of 1994/95, and the exceptionally large sea-level fall ($\sim$10.5 cm) during the winter of 1995/96 are in agreement with the interannual variation of the net heat flux. Thus, the amplitude intensification during 1995 can be explained to a large extent as domain-wide diabatic steric response. The contribution from adiabatic steric effects will be discussed later.

The altimetric signal in the northern half of the studied area has a distinct non-seasonal component whose variation resembles that of the NAO index (see Appendix C). The steric SLA_{St} and the Sverdrup SLA_{Sv} appear to explain regionally the non-seasonal component. The spatial pattern comparison of the steric SLA_{St} principal empirical mode and the wind speed's third empirical mode shows regional similarities (EOF analysis—see Appendix C), which might indicate a wind-induced net heat flux variation related to the NAO variation. At a very coarse scale, a zonal gradient is observed in the spatial patterns of both the Sverdrup SLA_{Sv} and the 'steric-corrected' altimetric SLA principal empirical modes. On the eastern side of the Iberian Basin in particular, the SLA_{Sv} magnitude is comparable to the altimetric SLA one. However, towards the MAR the altimetric SLA and Sverdrup SLA_{Sv} spatial patterns start to differ. Just west of the MAR, a comparable zonal gradient is again observed, although the SLA_{Sv} magnitude there is unrealistically high. The strong variations of the Mid-Atlantic Ocean's bottom topography are probably playing an important role in the barotropic response of the ocean, as suggested by Koblinsky (1990). The flat bottom assumption does not apply there and, as a consequence, it is difficult to assess the Sverdrup balance contribution to the total sea-level variance. Extending the investigation to the topographic Sverdrup balance case is expected to yield more realistic results. Besides the physical models used to explain that non-seasonal signal, it is worth noting the principal gradients characterising its spatial pattern. Their locations are along, or close to, two main currents: the eastward-flowing near-zonal Azores Current ($\sim$34°N) and the southward-flowing Portugal Current (off the Iberian Peninsula). Thus, part of their variability should be related to the NAO variability.

A local Ekman pumping response correlated with the steric-corrected signal also was found (a) in the northern part of the studied area, and (b) in the Eastern Canary Basin. The SLA time variation in the northern Iberian Basin resembles the time integral of the NAO-like empirical mode of the wind-stress curl (see Appendix C). Both correlated patterns in the north are characterised by dominant semi-annual variability. On the other hand, the SLA signal in the Eastern Canary Basin mainly exhibits an annual-scale variation. Since the two

wind sources (ECMWF and CERSAT) give quite different results and the accuracy of steric correction is questionable, we cannot draw definite conclusions from these results. In general, the contribution of the Ekman pumping to the steric signal in the studied area was inferred on the basis of scaling arguments. Thus, the results should be cross-validated by other studies.

Wind-induced sea-level changes were also found in the southern Canary Basin (south of $\sim 25^{\circ}$N) after 1995, which could be attributed to Ekman pumping response (between 20°W and 30°W) and to Sverdrup balance (west of 30°W). However, other baroclinic signals (waves) also could explain part of the signal and, therefore, modelling of the non-local (propagating) response will be necessary to achieve an accurate interpretation of the overall variability of the equator-ward part of the studied area.

The interannual variability consists of two distinct variations. First, a near-continuous interannual trend of sea-level rise, located in the central part of the area, but also—with a higher rate—on its southeastern side, while a rather weak sea-level fall is observed on the northwestern side (west of the MAR). SST data analysis showed that the SST interannual increase is consistent with the overall sea-level rise but not with the spatial tilt, which results from the differential trend between the northwestern and southeastern regions. The ratio between the linear trends of SLA and SST reaches its maximum close to the Gibraltar Straight, where the warm, high-saline Mediterranean water outflows into the Atlantic Ocean. However, assessing whether some of these changes are caused by an interannual trend of the Mediterranean fresh water/salt budget is not possible, since no monitoring data on the Mediterranean outflow are available. Besides the lack of in situ observations, this trend is most probably indicating water-density changes at interannual timescales in the Canary Basin. An increase of the ocean thermal content can be suspected in this area, since warming was revealed recently by analysis of repeated XBT lines (Stolley et al., 1999). Similarly, a southward migration of Labrador Sea waters along the MAR has been reported recently, which could contribute to a lowering of the sea level into the northwestern part of the studied area (Lorbacher and Kolterman, 1999). Nevertheless, a geographical extension of our study has revealed that this differential trend is part of an Atlantic Basin-wide variation with an elongated centre of action along the Gulf Stream and North Atlantic Current, while the subpolar Atlantic and the eastern subtropical and tropical Atlantic experience an opposite variation (not shown). Hakkinen (1999) has attributed this mode to the low-frequency changes of the North Atlantic meridional overturning circulation, which could be related to the NAO. Esselborn et al. (2000) found a noticeable correlation of this mode with the time integral of the NAO index, and assigned the overall variation to changes of the heat storage in the North Atlantic.

So, is the observed linear trend directly related to the North Atlantic Ocean's variability? And at which scale (regional- to basin-wide)? Recent analyses of the SST anomalies in the North Atlantic Ocean have revealed that a large-scale pattern occurs on interannual-to-decadal timescales (Deser and Blackmon, 1993; Kushnir, 1994; Hansen and Bezdek, 1996; Sutton and Allen, 1997), which is related to the atmospheric forcing by the NAO. This pattern has a tripole structure with almost zonally oriented anomalies in the subtropical and high-latitude SSTs being in phase (and with the NAO index, too) and mid-latitude being out of phase. Moreover, the SST anomalies are not stationary; they propagate along the path of the North Atlantic Current (e.g., Sutton and Allen, 1997; Visbeck et al., 1998; Krahmann et al., 2001). The spatial pattern of the principal mode of SST fields compares well locally with the spatial pattern of the principal empirical mode from an Atlantic Basin-wide EOF analysis, which spans a longer period (Seager et al., 2000; Visbeck and Krahmann, 2000). The near-linear time variation between 1994 and 1998 is commonly observed in both the time patterns of the local- and basin-wide analyses. However, the time-extended analysis reveals that the near-linear trend is confined only within the limits of our study's time window, and is not a long-term persistent feature.

The second distinct interannual variation corresponds to a significant temporal rise during 1995

with an average magnitude of ~ 3 cm, which is more pronounced in the central region (between the Azores and Madeira). Note that this fluctuation is the main spatial feature of both the (detrended) SLA and SST EOF's principal empirical modes (Fig. 11). Another minor area subject to this time variation is centred around the northwestern corner of our study area. However, this interannual variation is a rather local phenomenon in compared to the basin-wide trend mentioned above. An investigation based on analysis of non-filtered SLA time-series revealed that the initial rise start is quite sharp and takes place during the early winter of 1994/95. With the exception of the winter of 1995/96, all other winters are characterised by a sharp sea-level rise, but the temporal averaging applied smoothes these short events. These events occur in late autumn and early winter, suggesting a relation with the ocean's maximum net heat loss, which takes place during the same period of the year.

Analysis of the interannual variation of net heat loss (mentioned above when explaining the interannual amplitude variation in the annual cycle) supports the hypothesis of a domain-wide diabatic steric response. However, it does not explain the locally intensified response south of the Azores, and the recurrent feature (with the exception of the winter of 1995/96) of these season-specific events. The combination of wind-induced heat flux, momentum flux, and the region's surface circulation could be a plausible explanation. The EOF analysis of the wind speed during winter (December–March) yielded an empirical mode (25% of the total variance) whose variation is similar to the winter-only NAO index (not shown). The corresponding spatial pattern is quite similar to the spatial pattern of the altimetric SLA (Fig. 11a), but with negative magnitude, which means that the wind intensifies or decreases inversely to the NAO index. During the 6-year period, the wind speed minimum in the Azores region occurs in the winter of 1994/95. Thus, a wind-induced local reduction of heat flux could lead to a local reduction of the winter-to-early spring sea-level fall. Furthermore, examination of the local wind conditions south of the Azores region has shown that the seasonal variation of the predicted Ekman pumping SLA response is mainly characterised by a temporal rise in March. If we take into account that during early 1995, the wind-stress curl forcing was the strongest observed due to the highly positive phase of the NAO, the Ekman pumping effect would have been at its strongest during the 6-year period. The EOF analysis of heat storage in the upper ocean (200 m) based on temperature data (Scripps Institution of Oceanography, Joint Environmental Data Analysis Center) has confirmed a co-located anomalous heating of the upper ocean during 1995 (not shown), together with a downward displacement of the isotherms. However, in the Iberian Basin where the wind-stress curl change is much stronger (Fig. 15a), the observed response of sea level on an interannual timescale appears not to be analogously strong (Fig. 11a). Taking into account that only the local effects of atmospheric forcing are examined in our study, we suspect that part of the discrepancy found could be attributed to vorticity radiation by baroclinic waves. Another plausible explanation, among other factors, for the location of the intense SLA is that the region north of the Azores Current ($\sim 34^{\circ}$N), which extends from west of the Azores to Madeira, is a region of convergence. This recent result obtained by Zhou et al. (2000) was deduced after estimating the mean surface current in the region through the study of drifter observations in the Canary Basin between February 1992 and January 1995. Thus, the accumulation of more- or less-cooled surface waters in the Azores–Madeira region during the winter and early spring period can amplify the intense steric response in that region.

We should also note that Chambers et al. (1997), after estimating the interannual heat storage rates (HSR, November 1992–November 1995) by using TOPEX data and comparing the results with concurrent SST rates, have reported a region of large HSR and SST in the northeastern Atlantic, which is co-located with the one found in the empirical modes of the detrended altimetric SLA and SST (Figs. 11a and b). Their results are derived from a shorter (3-year) studied period, for which the temporal rise during 1995 tends to increase the linear trend and indicate higher rates of sea-level variation. More recently, Leuliette and Wahr (1999) have found a global-scale empirical

mode of SLA and SST, which is regionally quite similar to the empirical mode given in Fig. 12. Moreover, the time variation of the global mode also appears as an increasing near-linear trend (characterised as a 'secular trend' by the authors). Furthermore, in the North Atlantic, this global-wide mode has the most coherent spatial pattern. This mode is associated with thermal expansion, also.

6. Conclusions

Altimetric observations from the T/P and ERS-1/2 satellites were used with concurrent oceanic and atmospheric parameters (net heat fluxes, winds, SST) to investigate the large-scale sea-level variations and their relation with air–sea interaction processes in the CANIGO area. This area only comprises part of the eastern branches of the Atlantic subtropical gyre, which is expected to be subject to basin-wide fluctuations over a broad band of timescales. Nevertheless, based on EOF decomposition, a comprehensive analysis was performed to fully separate and identify correlated patterns between the observed sea-level variability and the possible forcing parameters. This led us to evaluate the specific large-scale ocean dynamic response in quite limited areas (off Portugal, in the vicinity of the Canary Current system, north of the Azores Current).

The seasonal oscillation of the sea level (with annual amplitude ~ 4.8 cm) in this subtropical northeastern part of the Atlantic Ocean appeared to be consistent with the steric-height variations derived from ECMWF net heat fluxes, although the magnitude of the calculated steric height does not entirely match the observed signal (explained variance $\sim 90\%$). The deviation, which is larger in the Canary Islands region, could be attributed mainly to inaccuracies of the net heat flux data used. Because of the uncertainty in the precise magnitude of the predominant heat-forced steric response, the contribution of wind forcing on an annual timescale was difficult to assess. Thus, the conclusions on the Ekman pumping response (with annual amplitude ~ 1 cm) in the eastern Canary Basin should be treated with caution. We observed a small, but significant, interannual variation of the annual oscillation's amplitude ($\sim \pm 0.7$ cm). Some evidence of connection with the interannual variations of net heat loss was noticed, although the contribution from heat advection cannot be neglected.

Apart from the dominant annually oscillating signal, the residual one was found to be related mainly to the NAO's variations. Distinct spatial gradients of sea level associated with this signal are co-located with the paths of the Azores and Portugal Currents. The wind-induced heat exchange and the barotropic Sverdrup balance (flat-bottom case) appeared to be a preferred explanation for this non-seasonal signal. Ekman pumping effects also were observed at the northern limits of the studied area. In particular, the signal in the northern Iberian Basin exhibits a time-integrated NAO-like variation. However, the NAO pattern is acting mostly at the northern latitudes (north of 34°N) and some evidence of wind forcing (either Sverdrup- or Ekman-modelled) was also found in the southern Canary Basin after 1995.

On interannual timescales the observed domain-wide tilt of the sea level appears to extend outside the limits of the studied area. Again, a sure explanation can be reached only by a comprehensive basin-wide study of the different processes. By assuming that the SST is an approximate indicator of the upper-ocean heat content, we can explain most of the sea-level variations (the long-term rise of ~ 0.5 cm/year and a temporal rise of ~ 3 cm during 1995) in the central region and in the southeastern side of the studied area as the result of a steric (i.e. diabatic) response of the Atlantic Ocean. The ratio (regression coefficient) between the two surface fields, wherever the spatial patterns of their principal modes are comparable, spans from 2 to 3.5 cm/°C. However, before the explanation based on thermal expansion/contraction can be accepted, it will be necessary to explore in situ data, as well. Moreover, part of the low-frequency SLA signal in the central and northeastern areas can be explained by the wind-stress curl changes on interannual timescales (Ekman pumping effects). The long-term trend appears to be part of an Atlantic-scale pattern of variability associated with the NAO (basin-scale response), whereas the

temporal rise during 1995 could be explained as the result of the NAO-related atmospheric forcing (local response). Thus, the NAO appears to play an important role in determining the studied area's sea-level variability across a broad spectrum of timescales, from intraannual and annual to interannual ones.

Acknowledgements

This study was supported by the European Union through the MAST-III CANIGO project (contract MAS3-CT96-0060). The ECMWF (European Centre for Medium-range Weather Forecasting) wind field dataset was kindly provided by the AVISO/Vent-Flux team at PREVIMAR, Météo-France. The scatterometer wind field was extracted from the CERSAT/IFREMER mean products database. The NAO index was obtained from the Climate Research Unit of the University of East Anglia. We thank Marie-Hélène Calvez, at CLS, who processed the SLA maps from T/P and ERS-1/2 altimeter data. We are grateful to Alexander Rigas at the Demokritos University for his assistance during the manuscript preparation. We also thank the reviewers for their helpful comments.

Appendix A. Coefficient of thermal expansion

We test various ways of estimating α, based on data from the upper 200 m of the ocean, which includes the oceanic layers with noticeable seasonal variability of temperature T and salinity S (the

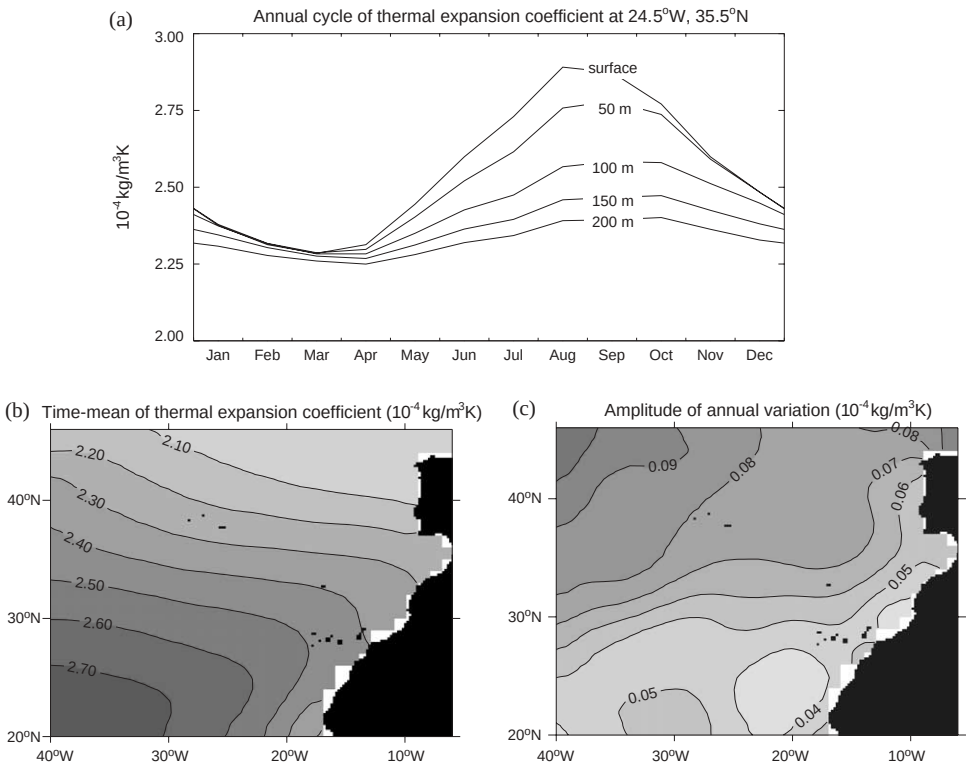

Fig. 13. Variability in time and space of the thermal expansion coefficient: (a) the annual cycle at 24.5°W/35.5°N, taking into account temperature and salinity data either from only the ocean surface, or from the upper 50, 100, 150, and 200 m, (b) the geographical variation of the time-averaged values within the studied area using temperature and salinity data from the upper-ocean layer (200 m), and (c) the corresponding amplitude variation (FFT-based harmonic fit) of the annual cycle.

magnitude of the variability of each variable decreases with depth). The thermal expansion coefficient α is calculated for each depth level with monthly S and T values provided by the WOA94. Then, a mean α value is computed as a weighted average of the monthly α values at each level. Weights are given as half the upper and lower layer thickness. The sensitivity study was carried out by computing a mean α coefficient averaged over different ocean depths. The mean and the range of these α values decrease with the number of layers (see Fig. 13a), and so does the steric-height response to net heat flux forcing. By assuming that the 200-m upper layer is where the ocean thermally interacts with the overlaying atmosphere, the resulting α coefficients range from 2.0×10^{-4} to $2.8 \times 10^{-4}\,\mathrm{kg/m^3\,K}$. Larger values are found in the southwestern Canary Basin and lower ones in the Iberian Basin (Fig. 13b). The α coefficient exhibits seasonal to temporal variations, depending on the upper ocean T and S characteristics. Fig. 13c shows the annual cycle amplitude of the α coefficient, ranging over the area between 0.04 and $0.10 \times 10^{-4}\,\mathrm{kg/m^3\,K}$.

Appendix B. Sensitivity of results to wind data source selection

The ECMWF wind data were used throughout our study. The results obtained can be affected by the accuracy of these wind data. To assess their accuracy, we computed simple statistics (mean field and time variability) and compared the results with the corresponding ones obtained from ERS-1/2 scatterometer wind data, which are provided

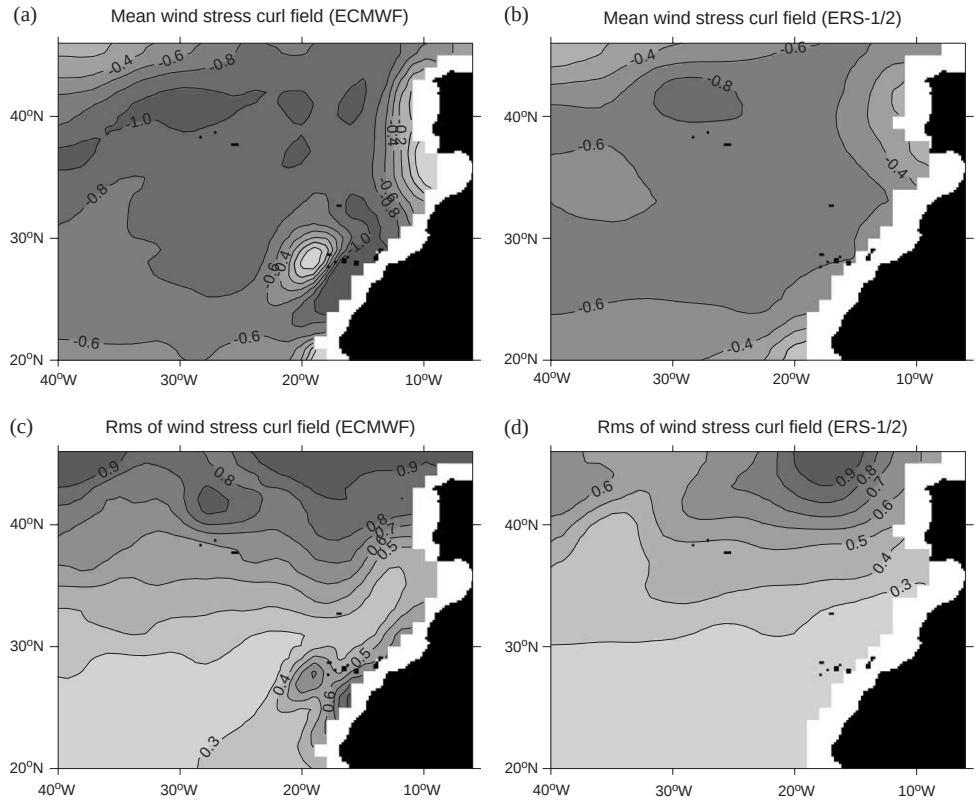

Fig. 14. The time-averaged field of the wind-stress curl during the 1993–98 period and the geographical distribution of the variability (expressed in rms) of the 3-month averaged wind-stress curl time series as derived from the ECMWF (a, c) and the ERS-1/2 (b, d) datasets. Contour intervals are $0.2 \times 10^{-7}\,\mathrm{N/m^2}$ (mean field) and $0.1 \times 10^{-7}\,\mathrm{N/m^2}$ (rms).

by CERSAT (Centre ERS d'Archivage et de Traitement; weekly objectively analysed global wind field on $1^\circ \times 1^\circ$ grids). The ECMWF mean wind-stress curl field during 1993–98 is slightly more negative than the corresponding one in ERS-1/2 observations (Figs. 14a and b). The most noticeable difference appears east of the Canary Islands in the form of a dipole with a distinct positive centre, which is observed only in the ECMWF data (Fig. 14a). We suspect that this dipole is unrealistic because the corresponding calculated Sverdrup transport (not shown) would produce a zonal front at 29°N within the general circulation of the subtropical northeastern Atlantic gyre circulation, which has not been observed. Moreover, the rms of the 3-month averaged wind-stress curl field is higher in the ECMWF analyses than in the ERS-1/2 data (Figs. 14c and d). This characteristic can result in weaker wind-induced ocean circulation variations, if one uses instead the ERS-1/2 wind data in the calculations. In the Canary Islands, the rms of the ECMWF is again much higher than the ERS-1/2 observations. This local discrepancy further supports the argument that the ECMWF model output for that region should be carefully cross-validated with other wind data sources.

Appendix C. Wind variability and the North Atlantic Oscillation

The northern part of the area investigated is located close to the southern centre of action of the dominant atmospheric teleconnection pattern of the Atlantic sector. This atmospheric variation is known as the North Atlantic Oscillation (NAO), and its impact on the North American and European climate has been recently investigated (e.g., Hurrell, 1995). A measure of this phenomenon, namely the NAO index, is usually defined as the difference of normalised sea-level pressure

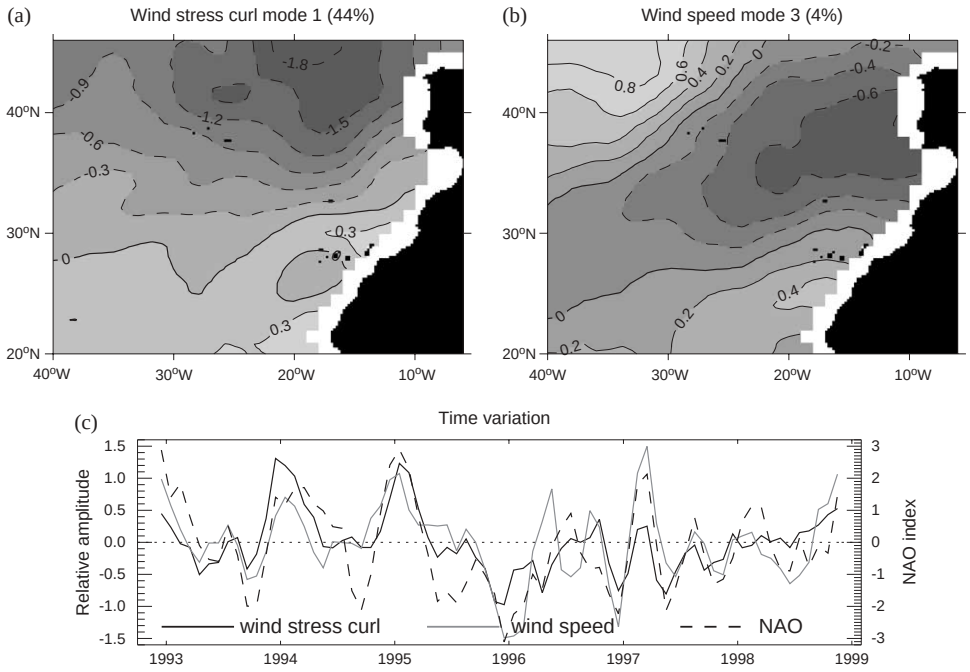

Fig. 15. Spatial patterns of (a) wind-stress curl (from ECMWF) and (b) wind speed (from CERSAT) of their respective empirical modes. For mode 1 (principal) contour intervals are $0.3 \times 10^{-7}\,\mathrm{N/m^2}$, while for mode 3 they are 0.2 m/s. The corresponding time variations are given in the bottom panel. A 3-month averaging was applied prior to the EOF analysis. The time variation of the NAO index, i.e. the normalised pressure difference between Gibraltar and southwest Iceland (3-month averaged), is also shown for comparison.

(SLP) anomaly between the subtropical (Azores or Western Iberia) and the subpolar (Iceland) Atlantic. The selection of these two regions is based on the strong anti-correlation of their respective SLPs (especially during winter), a fact that is also highlighted if an EOF analysis is performed on the North Atlantic SLP field (Trenberth and Paolino, 1981). To examine the relation of the wind-stress curl variability in the area with the NAO, we performed an EOF analysis on monthly values of wind-stress curl, each of them representing a 3-month average. The calculated first empirical pattern has a dominant pattern ($\sim$44% of the total variance) with a strong centre of action off northwestern Iberia, which extends up to the Azores, and a variation in time, which is strongly correlated ($r \sim 0.72$) with the time variation of the NAO index (Figs. 15a and c). The high negative (positive) values of the wind-stress curl (NAO) during the 1993/94 and 1994/95 winters, followed by the sharp rise (drop) to a positive (negative) value in the 1995/96 winter, are the main characteristics of the variation with respect to the mean state of the atmospheric fields (negative wind-stress curl and high SLP). In addition, the EOF analysis of the wind-speed field (provided by CERSAT) yields a principal empirical mode with a seasonal time variation ($\sim$77% of the total variance). In spite of the dominant seasonal fluctuation, a small part of the total variance ($\sim$4%), which corresponds to the third empirical mode, appears to be related to the NAO. The empirical mode's time variation is well correlated ($r \sim 0.69$) with the that of the NAO index (Figs. 15b and c). A description of the multi-annual variability of the wind-stress and wind-speed fields in the Atlantic Basin in relation to the winter-only NAO index variations can be found in the studies of Visbeck et al. (1998), Krahmann et al. (2001), and George and Saunders (2001).

References

AVISO User Handbook, 1996. Merged TOPEX/POSEIDON Products. AVI-NT-02-101-CN, Edition 3.0. Toulouse, France.

Centre ERS d' Archivage et de Traitement, 1994. ERS-1 Altimeter Products User Manual. Handbook C1-EX-MUT-A21-01-CN. Brest, France.

Centre ERS d' Archivage et de Traitement, 1996. Altimeter and Microwave Radiometer ERS Products User Manual. Handbook C2-MUT-A-01-IF. Brest, France.

Chambers, D.P., Tapley, B.D., Stewart, R.H., 1997. Long-period ocean heat storages and basin-scale heat fluxes from TOPEX. Journal of Geophysical Research 102 (C5), 10525–10533.

Chelton, D.B., Schlax, M.G., 1996. Global observation of oceanic Rossby waves. Science 272, 234–238.

Cipollini, P., Cromwell, D., Jones, M.S., Quartly, G.D., Challenor, P., 1997. Concurrent altimeter and infrared observations of Rossby wave propagation near 34°N in the Northeast Atlantic. Geophysical Research Letters 24 (8), 889–892.

Cromwell, D., Challenor, P.G., New, A.L., Pingree, R.D., 1996. Persistent westward flow in the Azores Current as seen from altimetry and hydrography. Journal of Geophysical Research 101 (C5), 11923–11934.

Deser, C., Blackmon, M., 1993. Surface climate variations over the North Atlantic Ocean during winter: 1900–1989. Journal of Climate 6 (9), 1743–1753.

Ducet, N., Le Traon, P.-Y., Reverdin, G., 2000. Global high resolution mapping of ocean circulation from TOPEX/POSEIDON and ERS-1/2. Journal of Geophysical Research 108 (C8), 19477–19498.

Esselborn, S., Miller, L., Cheney, R., 2000. Heat storage in the North Atlantic Ocean between 1992 and 1998 as estimated from satellite altimetry. AGU Chapman Conference on "The North Atlantic Oscillation", Orense, Galicia, Spain, 28 November–1 December 2000. American Geophysical Union, Washington, DC.

Ezer, T., 1999. Decadal variabilities of the upper layers of the subtropical North Atlantic: an ocean model study. Journal of Physical Oceanography 29 (12), 3111–3124.

Ferry, N., Reverdin, G., Oschlies, A., 2000. Seasonal sea surface height variability in the North Atlantic Ocean. Journal of Geophysical Research 105 (C3), 6307–6326.

Fukumori, I., Raghunath, R., Fu, L.-L., 1998. Nature of global sea level variability in relation to atmospheric forcing: a modeling study. Journal of Geophysical Research 103 (C3), 5493–5512.

George, A.E., Saunders, M.A., 2001. North Atlantic Oscillation impact on tropical Atlantic winter atmospheric variability. Geophysical Research Letters 28 (6), 1015–1018.

Gill, A.E., 1982. Atmosphere–Ocean Dynamics. Academic Press, San Diego, California.

Gill, A.E., Niiler, P.P., 1973. The theory of the seasonal variability in the ocean. Deep Sea Research 20, 141–177.

Hakkinen, S., 1999. Decadal Variability in sea level and its relationship to meridional overturning in the North Atlantic. WOCE North Atlantic Workshop, Kiel, 23–27 August 1999.

Han, G., Ikeda, M., 1996. Basin-scale variability in the Labrador Sea from TOPEX/POSEIDON and Geosat

altimeter data. Journal of Geophysical Research 101 (C12), 28325–28334.

Hansen, D.V., Bezdek, H.F., 1996. On the nature of decadal anomalies in the North Atlantic sea surface temperature. Journal of Geophysical Research 101 (C4), 8749–8758.

Hernandez, F., Le Traon, P.-Y., Morrow, R., 1995. Mapping mesoscale variability of the Azores Current using TOPEX/POSEIDON and ERS-1 altimetry, together with hydrographic and Lagrangian measurements. Journal of Geophysical Research 100 (C12), 24995–25006.

Hurrell, J.W., 1995. Decadal trends in the North Atlantic Oscillation: regional temperatures and precipitation. Science 269, 676–679.

Isoguchi, O., Kawamura, H., Kono, T., 1997. A study on wind-driven circulation in the subarctic North Pacific using TOPEX/POSEIDON altimeter data. Journal of Geophysical Research 102 (C6), 12457–12468.

Kelly, K.A., Singh, S., Huang, R.X., 1999. Seasonal variations of sea surface height in the Gulf Stream region. Journal of Physical Oceanography 29 (3), 313–327.

Knudsen, P., Andersen, O.B., Knudsen, T., 1996. ATSR sea surface temperature data in global analysis with TOPEX/POSEIDON altimetry. Geophysical Research Letters 23 (8), 821–824.

Koblinsky, C.J., 1990. The global distribution of f/H and the barotropic response of the ocean. Journal of Geophysical Research 95 (C3), 3213–3218.

Krahmann, G., Visbeck, M., Reverdin, G., 2001. Formation and propagation of temperature anomalies along the North Atlantic Current. Journal of Physical Oceanography 31, 1287–1303.

Kushnir, Y., 1994. Interdecadal variations in North Atlantic sea surface temperature and associated atmospheric conditions. Journal of Climate 7 (1), 141–157.

Le Traon, P.-Y., 1991. Time scales of mesoscale variability and their relationship with space scales in the North Atlantic. Journal of Marine Research 49, 467–492.

Le Traon, P.-Y., De Mey, P., 1994. The eddy field associated with the Azores Front east of the Mid-Atlantic Ridge as observed by the GEOSAT altimeter. Journal of Geophysical Research 99 (C5), 9907–9924.

Le Traon, P.-Y., Ogor, F., 1998. ERS-1/2 orbit improvement using TOPEX/POSEIDON: the 2 cm challenge. Journal of Geophysical Research 103 (C4), 8045–8058.

Le Traon, P.-Y., Nadal, F., Ducet, N., 1998. An improved mapping method of multi-satellite altimeter data. Journal of Atmospheric and Oceanic Technology 15 (2), 522–534.

Leuliette, E.W., Wahr, J.M., 1999. Coupled pattern analysis of sea surface temperature and TOPEX/Poseidon sea surface height. Journal of Physical Oceanography 29 (4), 599–611.

Levitus, S., Burgett, R., Boyer, T., 1994. World Ocean Atlas 1994. NOAA Atlas NESDIS, US Department of Commerce.

Lorbacher, K., Kolterman, K.P., 1999. Interannual and climate variability of volume, heat and freshwater transport estimates at ca. 45° N in the North Atlantic. WOCE Final Seminar, Bremerhaven, 28 April 1999.

Nerem, R.S., Haines, B.J., Hendricks, J., Minster, J.F., Mitchum, G.T., White, W.B., 1997. Improved determination of global mean sea level variations from TOPEX/Poseidon altimeter data. Geophysical Research Letters 24 (11), 1331–1334.

Reynolds, R., Smith, T., 1994. Improved global sea surface temperature analyses. Journal of Climate 7 (6), 929–948.

Seager, R., Kushnir, Y., Visbeck, M., Naik, N., Miller, J., Krahmann, G., Cullen, H., 2000. Causes of Atlantic Ocean climate variability between 1958 and 1998. Journal of Climate 13 (16), 2845–2862.

Stammer, D., 1997. Steric and wind-induced changes in TOPEX/POSEIDON large-scale sea surface topography variations. Journal of Geophysical Research 102 (C9), 20987–21009.

Stammer, D., Hinrichsen, H.-H., Kase, R.H., 1991. Can meddies be detected by satellite altimetry? Journal of Geophysical Research 96 (C4), 7005–7014.

Stolley, M., Sy, A., Ulrich, J., 1999. Long-term variability of the upper ocean thermal structure of the North Atlantic. WOCE North Atlantic Workshop, Kiel, 23–27 August 1999.

Sutton, R., Allen, M., 1997. Decadal predictability of North Atlantic sea surface temperature and climate. Nature 388, 563–567.

Tokmakian, R.T., Challenor, P.G., 1993. Observations in the Canary basin and the Azores frontal region using Geosat data. Journal of Geophysical Research 98 (C3), 4761–4774.

Trenberth, K.E., Paolino, D.A., 1981. Characteristic Patterns of Variability of Sea Level Pressure in the Northern Hemisphere. Monthly Weather Review 109 (6), 1169–1189.

Visbeck, M., Krahmann, G., 2000. Basin-scale sea surface temperature anomalies generated by North Atlantic Oscillation-like dipole forcing plus Gulf Stream advection. Nature, submitted for publication.

Visbeck, M., Cullen, H., Krahmann, G., Naik, N., 1998. An ocean's model response to the North Atlantic Oscillation-like wind forcing. Geophysical Research Letters 25 (24), 4521–4524.

Vivier, F., Kelly, K.A., Thomson, L., 1999. Contributions of wind forcing, waves, and surface heating to sea surface height observations in the Pacific Ocean. Journal of Geophysical Research 104 (C9), 20767–20788.

Wang, L., Koblinsky, C.J., 1996. Annual variability of the subtropical recirculations in the North Atlantic and the North Pacific: a Topex/Poseidon study. Journal of Physical Oceanography 26 (11), 2462–2479.

Wang, L., Koblinsky, C., 1997. Can the Topex/Poseidon altimetry data be used to estimate air–sea heat flux in the North Atlantic? Geophysical Research Letters 24 (2), 139–142.

White, W.B., Walker, A.E., 1974. Time and depth scales of anomalous subsurface temperature at ocean weather stations P, N, and V in the North Pacific. Journal of Geophysical Research 79, 4517–4522.

Willebrand, J., Philander, S.G.H., Pacanowski, R.C., 1980. The oceanic response to large-scale atmospheric disturbances. Journal of Physical Oceanography 10 (3), 411–429.

Wunsch, C., 1991. Large-scale response of the ocean to atmospheric forcing at low frequencies. Journal of Geophysical Research 96 (C8), 15083–15092.

Zhou, M., Paduan, J.D., Niiler, P.P., 2000. Surface currents in the Canary Basin from drifter observations. Journal of Geophysical Research 105 (C9), 21893–21911.